Egyptian Geophysical Society
EGS Journal, Vol. 17, No. 1, 187-203 (2019)

MAPPING THE BROAD BASEMENT STRUCTURAL LINEAMENTS, USING THE TILT ANGLE DERIVATIVES OF THE SATELLITE GRAVITY DATA AT THE VICINITY OF OWEINAT AREA, SOUTH WESTERN DESERT, EGYPT

A.S. HELALY
Department of Geophysics, Faculty of Science, Ain Sham University
Abbassiah, Cairo, Egypt. 11566, Ahmad.Helaly@sci.asu.edu.eg

تحديد الملامح التركيبية تحت السطحية بتطبيق بعض تقنيات كشف الحواف على بيانات الجاذبية غير الأرضية بالمنطقة المجاورة للعوينات بجنوب الصحراء الغربية، مصر

الخلاصة: الهدف الرئيسي من هذا البحث هو تحديد الملامح التركيبية تحت السطحية ، من خلال تطبيق بعض تقنيات كشف الحواف على بيانات الجاذبية غير الأرضية المتوفرة في منطقة الدراسة. وقد استخدمت بيانات الجاذبية غير الأرضية في الدراسة الحالية التي تهدف إلى رسم خرائط توضح الملامح التركيبية العامة (الصدوع) التي تشكل منطقة الدراسة.

معظم الحالات الشاذة في الطول الموجي ، بسبب تباين الكثافة المختلفة ، قد تمثل الملامح تحت السطحية القريبة. يمكن استخدام بعض التقنيات التفسيرية الجيوفيزيائية لتحسين الكشف عن هذه الأحرف التركيبية. ومن بين هذه التقنيات – المشتقات الأفقية والرأسية للمجالات المحتملة المقاسة. يمكن استخدام العديد من تقنيات كشف الحافة ، مثل الإشارة التحليلية ، والمشتق الأفقي الكلي لزاوية الميل ، والمشتق الأفقي العادي ، كذلك. يتفق معظم هذه الطرق في تحديد مثل هذه الاتجاهات التركيبية للمصادر المسببة لها تحت سطح الأرض ومواقعها الأفقية النسبية. ومع ذلك ، فإن دقة كشف الحواف تتناقص مع زيادة عمق الجسم المسبب.

تم تطبيق بعض هذه التقنيات للكشف عن هياكل التراكيب والبنيات القاعية في مدينة العوينات والمناطق المجاورة ، المنطقة الجنوبية الغربية ، مصر. إن تطبيق هذه الطرق على بيانات الجاذبية المتاحة أظهر بشكل أساسي هذه الإتجاهات التركيبية NNE-SSE و NW-SE و E-W و NNW-SSE.

ABSTRACT: *The main objective of this research is to delineate the subsurface structural lineaments, through applying some edge detection techniques on the available satellite gravity data in the study area. Satellite gravity data were used in the current study aiming to mapping of the general structural elements (faults) that govern the geometry of the studied area. And the latter was used in modeling the subsurface geological structures.*

Most short wavelength anomalies, due to different density contrasts, may represent near subsurface features. Some geophysical interpretive techniques can be used to improve the detection of such edge features. Among such techniques are the horizontal and vertical gradients of the measured potential fields. Many edge detection techniques, such as the analytical signal, total horizontal derivative of the tilt angle, and the normalized horizontal derivative, can be used as well. Most of these methods agree in identifying such structural trends of the subsurface causative sources and their relative horizontal locations. However, the edge detection resolution decreases as the causative body's depth increases.

Some of these techniques were applied for the detection of the basement structures within El-Oweinat and the nearby areas, Southwestern region, Egypt. The application of these methods on the available gravity data exhibited predominantly NNE-SSE, NW-SE, nearly E-W and NNW-SSE structural trends.

I- INTRODUCTION

The study of basement structures has some importance, because the basement setup reveals the tectonic situation and geologic history of any area. However, the sedimentary rocks gradually cover the different tectonic situations of the lineaments, tilted crustal blocks and ridges, which mask the underlying basement structures (Braitenberg et al., 2006). Alexander et al. (2003) also mentioned that structure analysis of the basement rocks can advance the understanding of the overlying sedimentary structures and the petroleum system. Also, the study of the basement structures, not only benefits the investigation of tectonic structures, but also helps to detect and explore the probable contained mineral resources.

The study area is located within the far Southwestern part of the Egyptian territory. It is bounded by the latitudes 22º00' N & 24º30' N and the longitudes 25º00' E & 30º00' E, which is covering a surface area of about 125,000 km^2, as shown in Figure (1). It is of some importance to study such far areas which could be promising areas for a subsequent study towards the future national purposes or projects. This is through delineating the deeper or low-lying basement relief, where could be of high potential for groundwater accumulation. Aeromagnetic and gravity surveys are necessary to establish the depth and shape of the basement rocks beneath the sediments in the southern part of the Western Desert. This knowledge is essential to a full understanding of the underground water reservoir and its future (El-Baz, et al; 1978). The current study is focused on delineating the broad structural trends using some techniques proposed by many authors, for example, Cooper (2003), Cooper and Cowan (2008), Cooper and Cowan (2009), and, Eshaghzadeh (2014). That is to get

an idea about the effect of such structural elements in configuring the subsurface section in the study area. Quantitative analysis of such effects will be addressed in another article.

II- GEOLOGY

The study area is, in general, of a sedimentary terrain, ranging in age from Precambrian to Quaternary, but with many missing ages in between. It is an arid region, with a few drainage lines, which are draining, in general, eastward. The area is of limited subsurface geologic information, because of the few drilled holes and the few previous geophysical and geological studies. Therefore, the main goal of this work is to recognize the subsurface basement structures, affecting the basement complex and its overlying sedimentary cover.

Interpretation of the gravity anomaly map and concluding the probable existed geological structural features prevailing in the study area, were carried out. This gravity map was filtered using some different techniques. Also, the Geosoft and Surfer (version 13) programs have been used for carrying out the required analytical operations, using the available map data sets.

II.1- General Geology of the Western Desert

The study area belongs to Al-Wadi Al-Jadid Governorate (Figure 1) within the Western Desert. In general, it is considered as a huge platform of sedimentary sequence, that is thinning southward, while thickening northward. Specifically, in the study area, the general higher topography is towards the West, while becoming of lower terrain towards the East, as shown in topographic map and its 3D view, (Figures 2 and 3), respectively.

The study area is a rocky platform of low altitude, due to the relative plain topography of the Western Desert. Therefore, most of the geophysical work can be performed easily along profiles in the E-W and N-S directions. Most of the sedimentary rock units composing the Western Desert are dipping smoothly northward. In general, the Western Desert is dominated by the Nubian Sandstone rocks at the south, Cretaceous- Eocene Limestone rocks in the middle, and Miocene Limestones towards the north. The eastern side of the Western Desert is characterized by relative smaller thicknesses of sedimentary rocks, due to the effect of faulting and folding.

Structurally, the Western Desert shows some folding features in the subsurface, which could be divided into three major groups (Said, 1962): N-S folding, NE-SW folding and NW-SE folding.

II.2- Geology of the Study Area (Oweinat and Gilf El-Kebir)

The known succession of strata, from older to younger is as follows: Precambrian basement of schists, granites,…etc.; Lower Paleozoic Sandstone; rhyolites; Lower Carboniferous, plant-bearing sandstones and the 'Nubian' Series of buff and brown false-bedded sandstone (El-Baz et al, 1978). In the Oweinat area and at Karkur Talh (to the north of Egypt-Sudan border, the upper surface of the rhyolite is smoothed and worn, and the overlying sandstones are similar in appearance to the Carboniferous bed at Karkur Murr (to the south of Egypt-Sudan border. No sandstone was found below the Karkur Talh rhyolite. If the rocks are the same, a definite interval must be allowed between the period of rhyolitic extrusions and the formation of Lower Carboniferous beds. This is the first indication of Paleozoic volcanism in the area, which implies the presence of contemporary hypabyssal and deep-seated acidic rocks. Burollet (1963) and Mahrholz (1965) worked on the nearby Libyan outcrops, where they were able to establish Cambro-Ordovician and Devonian clasticsections, both unconformably resting on the Precambrian gneisses. Also, a Devonian age is given to the clastics west of the Gilf El-Kebir, while the thick sandstone section forming the Gilf itself is believed to be of Jurassic-Cretaceousage. The Upper Cretaceous marine boundary was shifted several hundred kilometers further south of Abu Ballas twin hills.

II.3- History of the Stratigraphic Sequence

The oldest rock outcrops in the Oweinat - Gilf El-Kebir area are the Precambrian granites, granite gneisses and diorites, which form a northward-projecting outcrop of the main African Shield. During the Paleozoic, several intracratonic basins were formed within the shield and the sediments of this era filled those basins. One example of the intracratonic basins is the Oweinat – Gilf El-Kebir area (El-Baz et al, 1978). The general stratigraphic sequence of the area is demonstrated in Figure (4).

II.3.a- Palaeozoic rocks: In the Oweinat-Gilf El-Kebir area, three Paleozoic units were recognized, which have considerable areal extent. The basal unit is made up of ***hard quartzitic sandstone beds*** interbedded with highly consolidated conglomerate and syenite porphyry sheets. This unit assumes a thickness of approximately 20 meters and fills concavities and undulations in the Precambrian granite-granodiorite-complex surface between Gebel Oweinat and the Gilf El-Kebir area. A similar unit was recorded by Burollet (1963) on the western side of Gebel Oweinat, ***the Hassaouna Formation***, which is assigned to the Cambro-Ordovician interval. As to the middle and upper units of the Paleozoic rocks, the lower contact with the basement complex is highly kaolinized. The top surface is an erosional surface, which stretches northward for almost 130 km. It forms benches, which in the Oweinat area, are capped by approximately 20 meters of interbedded sandstone, phonolite and trachyte.

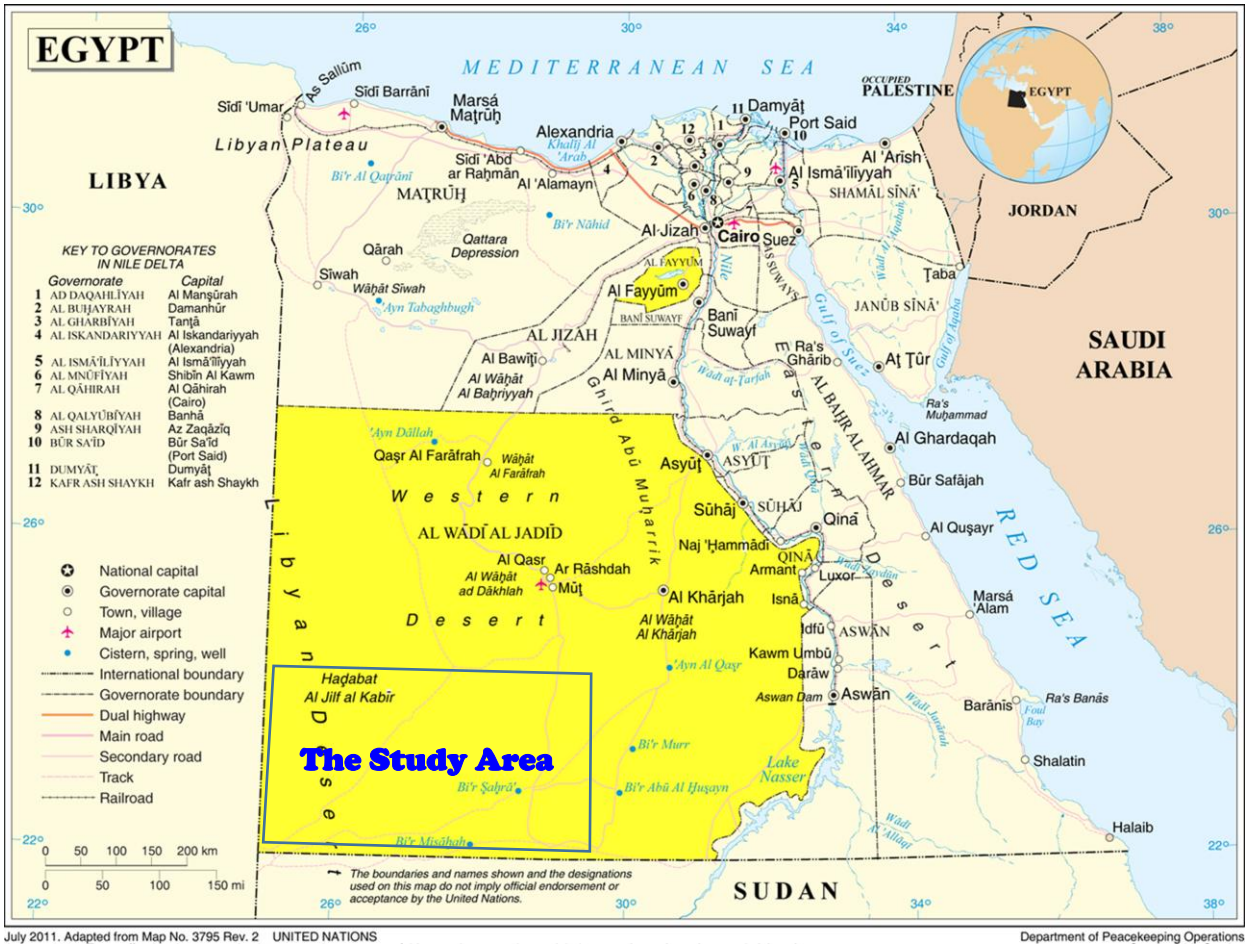

Figure (1): Al-Wadi Al-Jadid Governorate within which the study area lies.

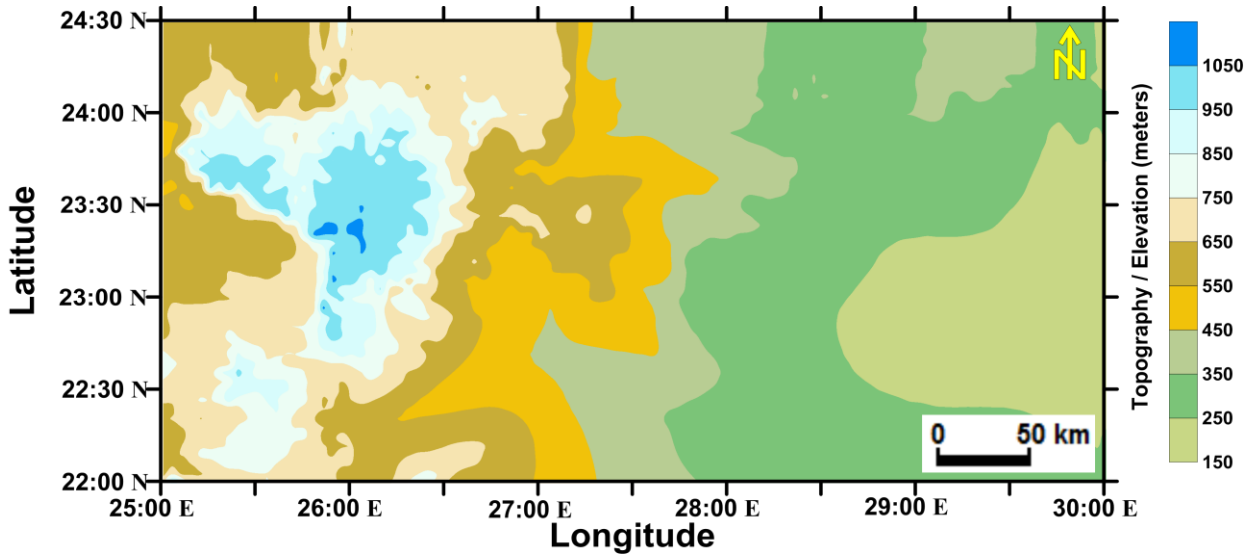

Figure 2: Topographic map of the study area.

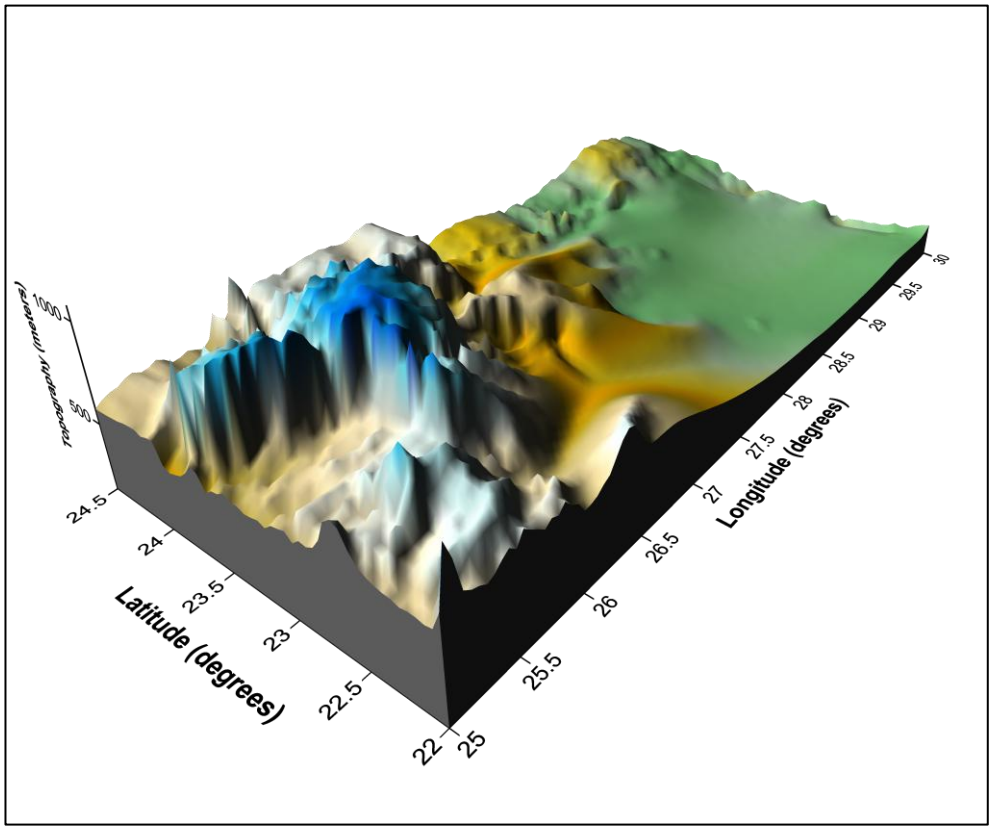

Figure 3: Three-dimensional view of the topographic map.

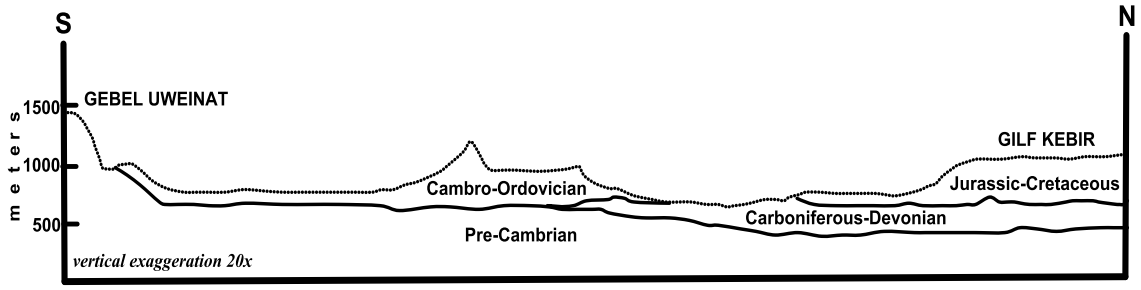

Figure 4: Geologic cross-section of the Gebel Oweinat-Gilf Kebir. Horizontal distance is 200 km (El-Baz; et al., 1978).

Northward and west of the Gilf El-Kebir, another unit of sandstone thickens gradually between the Cambro-Ordovician unit and the upper sandstone section. This middle unit is approximately 120 meters in thickness and forms the surface of the desert west of the Gilf El-Kebir, and the hills of Umm Ras and Abu Ras, near the Libyan border, atlatitude 23º 50' N. On the other hand, fossil plants from the upper unit in the Oweinat area assign it to Carboniferous.

After the deformation and plutonism of the Precambrian, the entire shield was uplifted and warped into broad intracratonic basins, in which the sequence of Paleozoic and volcanic rocks was accumulated. Although instability for some periods during the Paleozoic, as witnessed by the immense volcanic sheets and flows of that era and the uplifting of the Oweinat high trending NE-SW, no serious deformation has occurred since then (El Ramly, 1972).

II.3.b- Mesozoic rocks: The Gilf El-Kebir is made up of a thick sandstone unit, which unconformably overlies the Paleozoic section. The lower contact is kaolinized, while the top of the Gilf is characterized by a very hard quartzitic wall-like bed of three meters thick. The sandstone is of variable colors, showing wide textural and lithological variations. To this stratum; the name 'Gilf Sandstone' is here given. At the northeastern corner of the Gilf Plateau, clays intercalate the upper part of the sandstone section, which yields Upper Cretaceous fossils, comparable to the Dakhla and Duwi Formations, in the Kharga-Dakhla oases stretch. It is evident that, the Gilf Sandstone is comparable to the Nubian and the subsurface sandstonesection in the area of the oases. This subsurface section is considered Jurassic by Helal (1966),

Kedves (1971) and Saad & Ghazaly (1976). It thus seems feasible to assign the Gilf Sandstone to the Jurassic at the base and to the Upper Cretaceous at the top. The Upper Cretaceous Nubian Sandstone covers a great tract of the whole country south of the Kharga depression. It adjoins southwards of Bir Tarfawi and Bir Sahara against either the basement rocks or Paleozoic sandstone to the west.

II.3.c- Cenozoic (Quaternary) Rocks: A huge patch of Quaternary deposits has been recently mapped from the Bir Sahara-Bir Tarfawi area and further south, encompassing nearly 10 000 km^2. Lacustrine diatomite, limestone, carbonaceous silt and old sand dunes are the main types of sediments associated with the cultural remains of Upper Acheulean to Final Acheulean, Mousterian, Aterían and Historic ages (Wendorf, 1977).

II.4- Structural Setting

The general flatness of the Western Desert of Egypt is its most striking feature. Rock beds are nearly horizontal and only in rare cases, significant angles of dip can be noticed (Figure 5), e.g., at Karkur Talh (Oweinat), where several short E-W faults exist. The main faults in this part of the desert are normal gravity faults, including the Gilf fault, which extends about 150 km in a NNE direction on the western side of the Gilf El-Kebir; the Kemal fault, which is also 150 km long and trends in a NW direction along the western Gilf; and the Tarfawi fault, which skirts the western side of the Tarfawi igneous mass and runs over 220 km in a NNE direction. The distribution of the basement rocks, and the type and thickness of sediments, reflect several phases of structural development. Of importance are the two main igneous bodies at Oweinat to the west and at Tarfawi to the east. Between these two main masses lies the thick clastic section of the Gilf Sandstone indicating a basin of significant depth and continuation.

The Lower Palaeozoic sediments are poorly represented in the Oweinat area, while the Devonian-Carboniferous are better developed and show evidences of being slightly folded. This folding and the igneous intrusions may indicate post-Carboniferous orogenic movements, that resulted in the Oweinat high. The configuration of the Gilf basin is bounded eastward by the Tarfawi high. Because the sediments within the Tarfawi high are mostly of Cretaceous age and younger, it appears that the rise of the basement was initiated during a much later date than that of the Oweinat high. The only igneous rocks associated with this later movement are the basalts of Cretaceous-Oligocene age. Northward, extrapolation of these highs and lows makes it obvious that, the Tarfawi high trends north-northeast to join the Kharga swell. The Gilf basin, which assumes nearly the same trend, is believed to be a southern extension of the Dakhla basin, while the Oweinat high, also of the same trend, is mantled by the thick cover of the Great Sand Sea to the north. The fact that the western part of the area had been very active during the Late Paleozoic-Early Mesozoic whereas the eastern part shows signs of being unstable during the Cretaceous and Early Tertiary points to an eastward shift of tectonism with time.

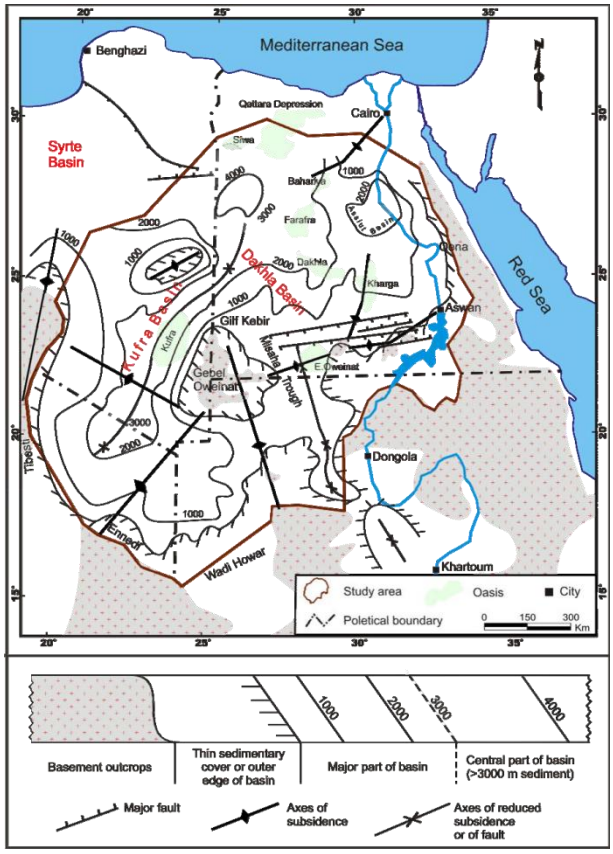

Figure 5: General structural framework of the NSAS, adapted from Klitzsch (1984), Klitzsch and Wycisk (1989)

II.4.a-The Surface Geological Units encountered within the study area are identified from the surface geologic map of Egypt, as shown in Figure 6.

III- GEOPHYSICAL WORK

Horizontal and vertical derivatives of the potential field anomaly data have been used for many years to detect the subsurface geologic inferences. Studies of edge recognition techniques have demonstrated that, the extreme point of the first horizontal derivative and the zero point of the first and second-order vertical derivatives correspond to the edge of the vertical fault (Cordell and Grauch, 1985; and Hood and Teskey, 1989).

Cordell and Grauch (1985) introduced some techniques to locate the horizontal positions of density or magnetization contrasts. Also, Hansen et al. (1987) used the magnitude of the horizontal gradient and the analytical signal to enhance the detection of edges and dips in gravity data. Cooper (2003) has developed a sun-shading technique, which is a directional filter to enhance the features in certain directions and suppress the linear features, which are perpendicular to the desired directions. Determining the locations of the subsurface magnetic bodies was done through the tilt angle technique, which was developed by Miller and Singh (1994).

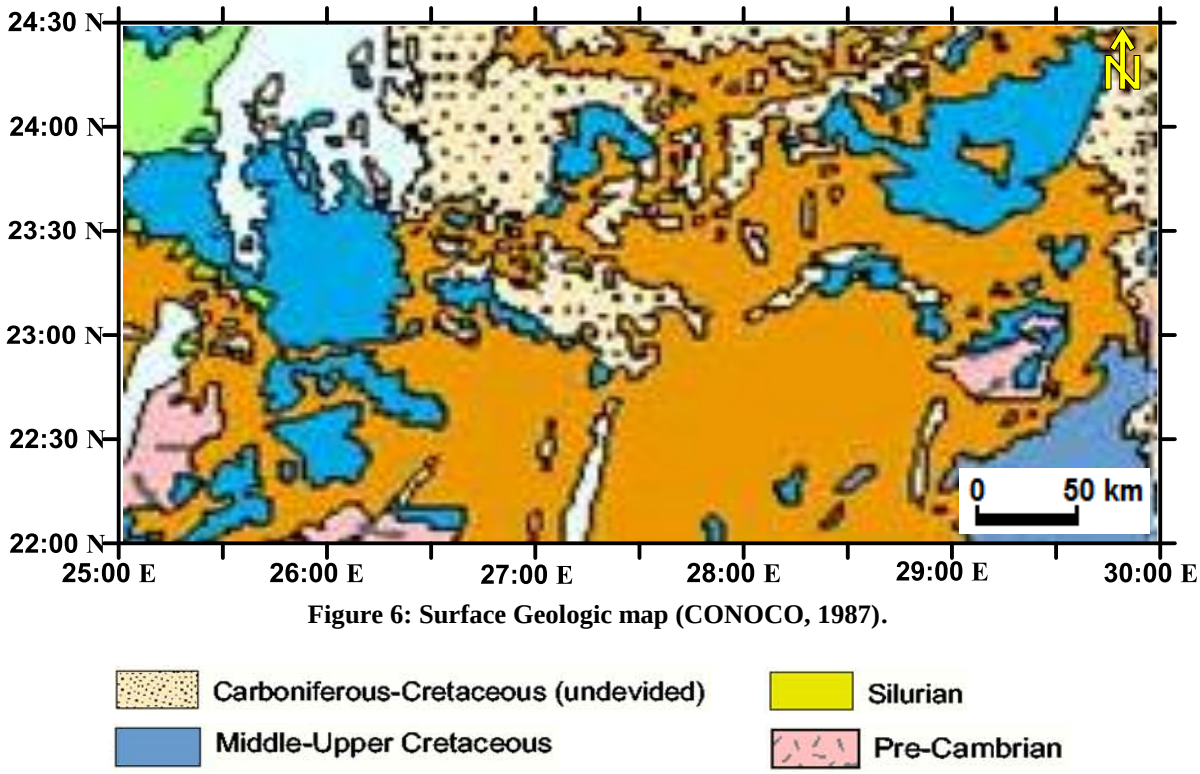

Figure 6: Surface Geologic map (CONOCO, 1987).

Verduzco et al (2004) improved the use of this technique to be used with gridded data, through the use of the total horizontal derivative in the tilt angle technique. In the current study, two techniques have been used, the Tilt Angle Map (TAM) and the Enhanced Total Horizontal Derivative of the Titl Angle (TA-THDR).

III.1- Gravity Data

Gravity anomalies are considered the results of the subsurface geologic inferences of different shapes, densities and depths. Linear anomalies are of special importance to the geophysicists, where they may reflect the presence of buried fault elements, or rock contacts or other tectonic or geological features. The fault elements always disrupt the continuity of the subsurface geological units, that of different densities and play a crucial role in the potential field data interpretation. Great deal of previous work has been done for detecting the structural edges from gravity data.

Due to the lack of ground gravity data for most portion of the study area, the data that were mainly used in this study are the Satellite gravity data derived from (Sandwell and Smith, 1997) and confirmed through (Bonvalot et al, 2012, BGI). The Satellite gravity data were used in the present study for some plausible aspects, for example: in case of areas where no ground data are available, their low cost (almost FREE), good areal coverage, and the ease to use, where the satellite data are usually obtained as gridded data.

Many authors used the Satellite-derived data in their studies. For example, McGinnis et al (1979), Hackney and Featherstone (2003), Trung et al (2004), Aboulela (2012), Ana et al (2014), Alkdagry (2015), and many others. Among those authors, Aboulela (2012) used the Satellite Gravity Data to study the tectonic settings of the northern Egyptian continental margin, and Alkdagry (2015), used the Satellite Gravity Data through the study over the Melut Basin in Sudan.

For checking the reliability of the used Satellite gravity data, they carried out comparisons (along some profiles in their work) between the obtained Satellite data and the gained gravity data from the marine survey (Aboulela; 2012), as shown in Figure (7), or with the measured ground gravity data (as Alkdagry, 2015), as shown in Figure (8). They found out that, the Satellite data showed only minor deviations with acceptable high matching between the Satellite data and the marine or the ground gravity-surveyed data of the studied areas, as shown in the figures below (Figures 7 &8).

Also, due to the lack of the gravity data in the study area, the author compared the Satellite data in other different surrounding areas, where the gravity data were available from the General Petroleum Company (GPC, 1984). Visual inspection showed only minor discrepancies between the gravity contours distribution between the GPC gravity maps and the Satellite gravity data.

For the current study, the Satellite gridded gravity data were originally obtained, as free air anomaly (FAA) data, as shown in Figure (9), together with the elevation data for each point. This combination of data was used to compute the Satellite-derived Bouguer Anomaly (BA) values for each gridded point in the study area.

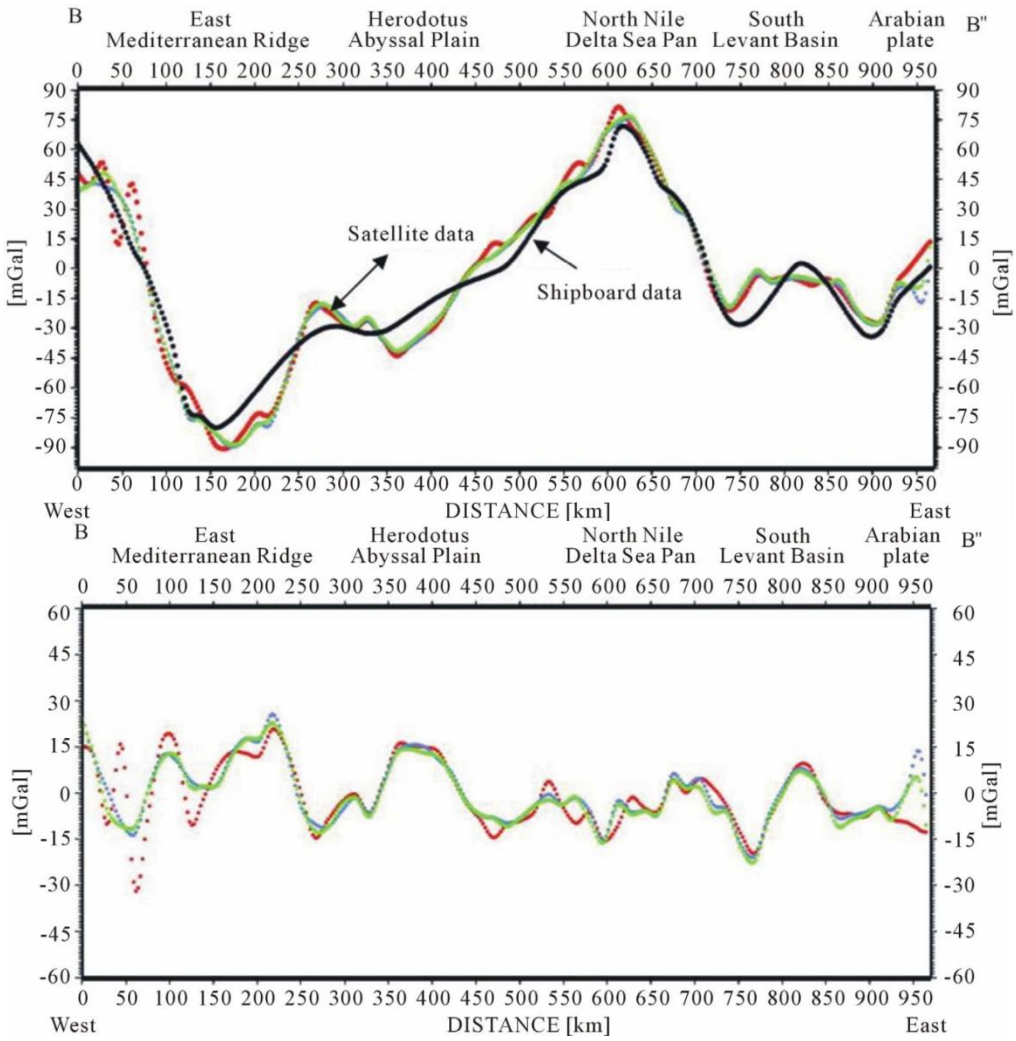

Figure 7: A comparison of the shipboard gravity data with the satellite gravity data along profile B-B"(Aboulela; 2012).

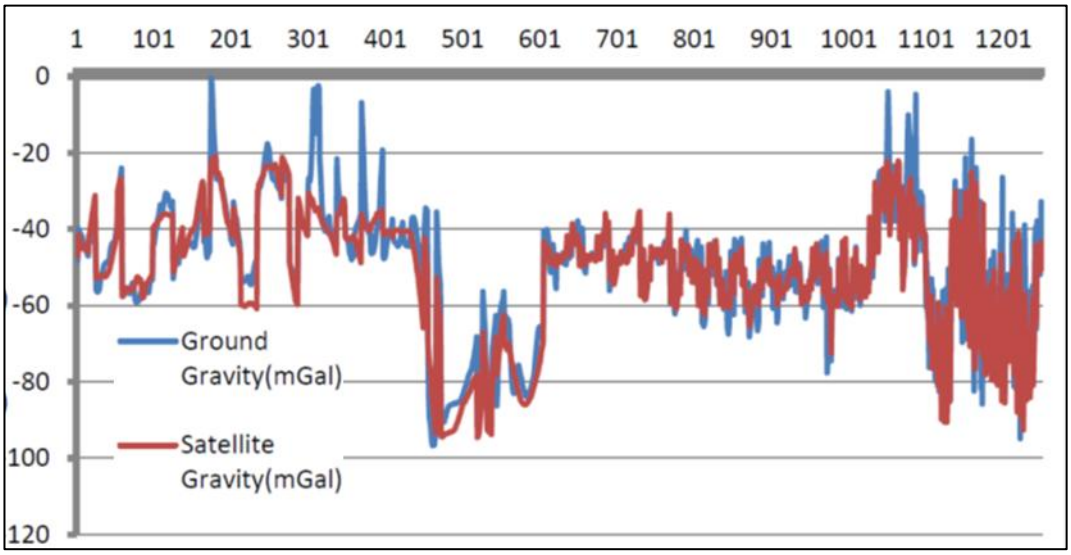

Figure 8: Comparison between the satellite and the ground gravity (Alkdagry; 2015).

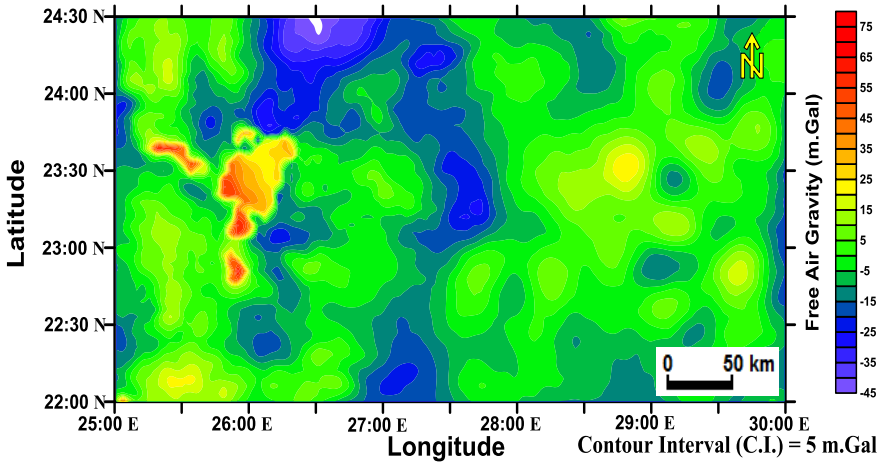

Figure (9): Free air gravity anomaly map.

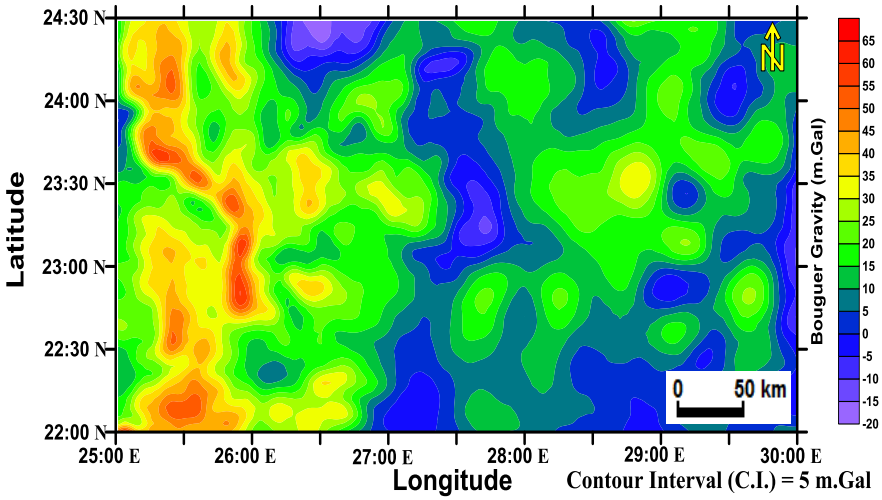

Figure 10: Satellite-derived Bouguer gravity anomaly map.

The theory about the Bouguer anomaly calculation from the gridded data of the free air anomalies and topography (or bathymetry) data can be summarized in a few steps as follows. First, correction of the Bouguer slab (Bullard A), which approximates the topography (or local bathymetry) with a plate of infinite lateral extension of constant density and thickness equal to the elevation of the point with respect to the sea level. Second, carrying out the curvature correction (Bullard B), this replaces the Bouguer plate by a spherical layer of the same thickness and surface. Third, performing the topographic correction (Bullard C), this deals with the effects of the surrounding topography above and below the station (Ana et al, 2014).

Then, the Bouguer Anomaly was computed using a FORTRAN program FA2BOUG developed by (Fullea et al, 2008), that calculates the Bouguer anomaly for land (and sea) grids. The input is sets of global grids of free air gravity anomalies and elevation (or bathymetry). The program calculates the corrections Bullard A, Bullard B and Bullard C, producing the needed Bouguer Anomaly data.

For the current study area, Figure (10) illustrates the obtained Bouguer gravity anomalies distribution that was generated using the kriging or minimum curvature (gridding) method to interpolate the data with a grid interval of 1 km × 1 km. The obtained Bouguer gravity anomaly displays several anomalous features of varying trends and amplitudes. In general, higher gravity values range from 15 up to slightly higher than 45 m.gal are within the western half of the gravity map, while lower gravity values range from less than 0 up to about 25 m.gal within the eastern half. The NW high elongated trend anomaly dominates, which reflects the Gilf El-Kabir structural high. There is another general N-S high anomaly. In the central part of the eastern half, the anomaly is relatively stronger (about +25 mGal) than the surroundings. Obvious NE trend can be seen, with some parallel smaller highs and lows. This gives the area the characteristics of some depressions related to uplifts in the general N-S and NE-SW extending gravity high and gravity low, that lie generally in parallel.

III.2 Steps of Methodology:

III.2.a- Residual Separation using the Polynomial Procedure:

The gravity and magnetic data represent a combination of the effects from the deeper and shallower causative sources. Anomalies with long wavelength (large width) are generated due to deeper sources, while short wavelength anomalies are due to shallower sources. Different techniques can be used for isolating the residual short wavelength from the regional trend long wavelength component. The regional-residual isolation based on polynomial fitting was proposed by Beltrao (1991), in which the coefficients are determined through a procedure of iteratively re-weighted least squares solutions. By successively assigning small weights to large residuals, their influence in the fitted regional is minimized, regardless of the "true" residual anomalies signs. It is a process that is insensitive to small departure from the idealized assumptions, for which the estimator is optimized.

Also, Abdelrahman et al. (2003) presented a procedure to select the optimum polynomial order, based on the correlation between the residuals of successive orders. It is concluded that the success of this method depends on the accuracy with which the residual anomaly is separated from the observed gravity anomaly. The residual gravity map is important in defining the geological structures and boundaries, which are targets of geophysical exploration. It is noted that, polynomial fitting (trend surface analysis) provided the best numerical approach. Therefore, it is more appropriate to compute from a gridded data, the best fit smooth surface using the least-squares polynomial fitting order and then remove the regional background.

The residual gravity map will be useful for the determination of the thickness of the basins and the study of the underlying depth-to-basement variations. In general, it will also be convenient for tectonic studies, anomaly transformation and mineral exploration.

The mathematical background of this regional-residual isolation technique can be reviewed from many textbooks and research papers. The author tried to solve a number of normal equations of the least squares problem. Their solution yields the unknown coefficients (c_1, c_2, c_3) of the equation:

$$[T(\mathbf{x},\mathbf{y}) = c_1 + c_2\mathbf{x} + c_3\mathbf{y}] \quad (1)$$

By which, the regional can be estimated at any gridded station of a certain **"x"** and **"y"** coordinates.

In this method, the regional and residual fields are represented by low and high order surfaces, respectively. The observed gravity anomaly is approximated by a power series. The regional field g_r along the x-axis can be represented by:

$$g_r = a^0 + a^1 x + a^2 x^2 + a^n x^n \quad (2)$$

where; **"n"** is the order of the polynomial being used to approximate the regional field.

The coefficients are evaluated using the principles of least squares and the trends of different orders (**n**) are computed. One of the low order trend, (say 2, 3, …) is selected as the regional field, and its difference from the observed field is the residual field. However, the selection of the order of polynomial (**n**) to represent the regional field is quite arbitrary, and depends considerably on the experience of the interpreter.

If the depth to the shallow sources is known in certain cases, for example, from the previously-studied seismic profiles or borehole information…etc, some constraints on the order of polynomial can be imposed, that will provide the right magnitude of the residual field at these points.

Accordingly, **The first step**: was the computing of the residual gravity anomaly by removing the second order polynomial surface from the Bouguer anomaly map. The degree of polynomial usually increases with increasing in the size of survey area. The second order polynomial fitting, based on the least square, was adopted in separating the regional and residual fields in the Bouguer gravity anomaly map of the study area. The Bouguer anomaly data was gridded using the Surfer (13) program, based on gridded data at approximately 1 km interval. The gridded data now has a uniform distribution of observation points, on which the polynomial fitting technique was applied.

The obtained regional map is shown in Figure (11). Figure (11) shows a second order polynomial of the regional field, which almost coincides with the smoothly varying field drawn, based on the visual inspection, as discussed above. In this Figure, the regional field shows gravity "high" towards the west and a gravity low towards the east, where the regional being fitted to the data is a two-dimensional second degree polynomial surface in the form:

$$y = 1.8403x^2 - 106.37x + 1545.6, \quad \textit{with } R^2 = 0.8921 \quad (3)$$

Then, using the obtained regional map, the residual map (Figure 12) is produced by subtracting the obtained regional data from the whole Bouguer anomaly map data.

Also, the residual causatives within the basement rocks were delineated, as shown in Figure (13). The anomalies did not show much variation within the basement rocks. This reflects the more relative homogeneity within the basement rocks' lithological characteristics, except in some places, that show the dislocations existed within the basement rocks.

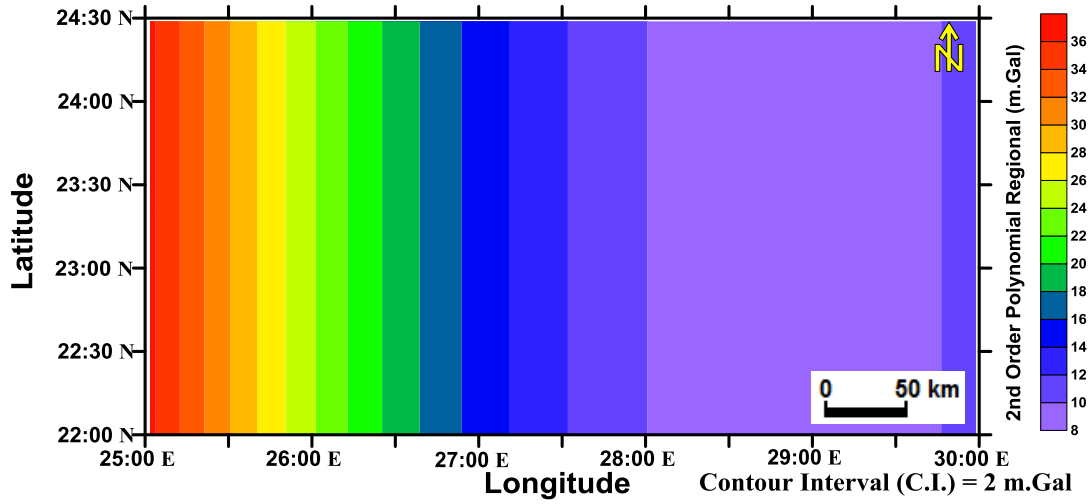

Figure (11): Regional gravity field exhibiting general N-S Trends.

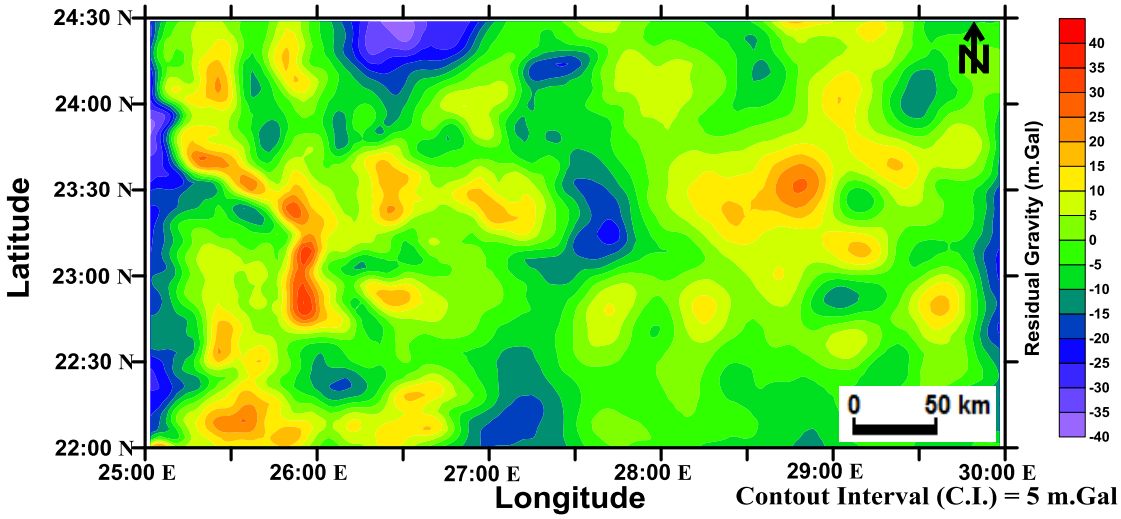

Figure (12): Residual gravity anomaly map computed by removing a second order polynomial surface (regional) from the Bouguer gravity anomaly map (within the sedimentary section).

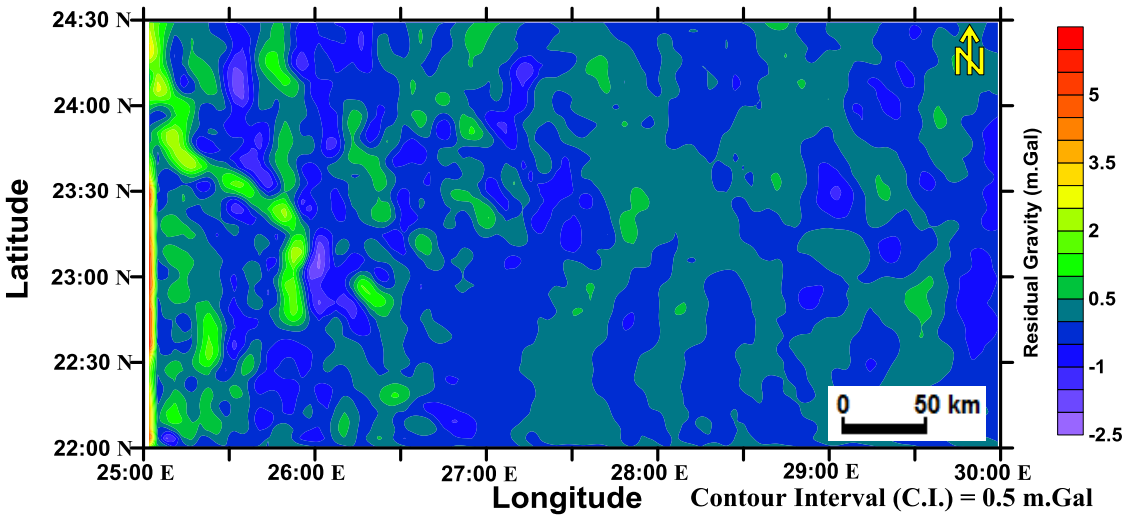

Figure (13): Residual gravity anomaly map computed by removing a second-order polynomial surface (regional) from the Bouguer gravity anomaly map (within the basement rocks).

III.2.b- First Vertical Derivative

Usually, the derivatives are used to sharpen the edges of anomalies and to enhance shallow features. It is stated that, the vertical derivative map is much more responsive to local influences than to broad or regional effects and therefore tends to give sharper picture than the map of the total field intensity. Thus, the smaller anomalies are more readily well-seen in area of strong regional disturbances.

In fact, the first vertical derivative is used to delineate the high frequency features more clearly where they are shadowed by large amplitude, low frequency anomalies.

From GEOSOFT Inc., 1996:

$L(r\} = r^n$, with: n is the order of differentiation.

The First Vertical Derivative (FVD) can be used to delineate the anomalous source's boundaries while limiting the high frequency amplification. The FVD can be calculated in the frequency domain by using the similar Fourier transform pair.

The concept of calculating the first vertical gradient is that, the surface ground data can be continued to a few centimeters above the surface. Then, calculating the gradient by subtracting the up-warded resulted data, from the ground surface data and dividing the difference by the height difference. Relation used for the upward continuation is based on the Fourier Transform method (Grant and West, 1965).

Accordingly, **The second step:** the first vertical gradient of the residual gravity anomaly was calculated using the Fast Fourier Transform (FFT) algorithm developed by Gunn (1975) and the results are illustrated in Figure 14, (*values are multiplied by 1000*).

III.2.c- Upward Continuation

Since short-wavelength noise, may exist in the obtained first vertical derivative data, due to different reasons (e.g. gridding artifacts, cultural noise, in general,…etc), that may interfere with the geologically meaningful lineaments, and is magnified when the subtle and short-wavelength anomalies are enhanced.

It is better that, these noises should be suppressed before proceeding in later work steps. For these noises suppression, some techniques can be considered, such as band-pass wavelength filtering, slight upward continuation, or smoothing with convolution filters. Band-pass filtering requires assuming the cut-off wavelengths, can smear the separation due to the non-vertical filter roll-off, and can contaminate the data by Gibbs ringing. By experimentation, upward continuation (usually by one cell size or at least its fraction) was found to be the most effective way for the gravity data noise cancelling in the study area.

Upward continuation uses wavelength filtering to simulate the appearance of potential-field maps, as if the data were recorded at a higher altitude. Short wavelength anomalies are suppressed preferentially.

Among the advantages of the upward continuation, the large-scale regional anomalies due to deep-seated features pattern can be revealed. Also, the main orientation of geologic features in the subsurface is revealed by the orientation of potential-field anomalies in the upward-continued maps.

Accordingly, **The Third Step** was estimating the upward continuation of the 1st vertical derivative (1st V.D.) field, that is to reduce the noise effect of the 1st V.D. response. The upward continuation was performed at two higher levels above the earth's surface and the results obtained were presented in Figure (15) (for the lower altitude) and Figure (16) (for the higher altitude), (*values multiplied by 1000*).

III.2.d- Tilt Angle

Usually, gravity maps are used to locate the geologic contacts and the boundaries of geological formations. These maps have signals of different amplitudes, that originate from sources with different geometries, located at different depths and with different density properties. Long ago, the vertical derivatives have been used to delineate the edges in gravity and magnetic field data (Evjen, 1936; Hood and Teskey, 1989 and Thurston and Smith, 1997). But also, in recent years, many meritorious authors demonstrated the use of the Tilt Angle (TA) technique in the edge detection of the subsurface anomalous features and also other improved methods have been introduced. For instance, the tilt angle (TDR) (Miller and Singh, 1994), the Theta map (Wijns et al., 2005), the total horizontal derivative of the tilt angle, as an edge detector (THDR) (Verduzco et al., 2004), the horizontal tilt angle (TDX) (Cooper and Cowan, 2006), the balanced analytic signal (Cooper, 2009) and the normalized horizontal derivative (Ma and Li.,2012).

Figure (17) shows that the tilt angle (ϕ) concept. A map of (ϕ) can therefore be considered an image of the tangent of the angle.

The geological model illustrating the geological contact or fault (modified from Klingeleet al., 1991) is shown in Figure 18.

Oruc (2011) has inferred that, the tilt angle (ϕ) for a vertical contact model (=90°) can be written as:

$$\phi = \tan^{-1}\left(\frac{x-x_0}{-(z-z_0)}\right) \qquad (4)$$

If z = 0, as the observation plane, $\phi = \tan^{-1}\left(\frac{x-x_0}{z_0}\right)$, where the value of the tilt angle equals"zero" radians at the measuring point ($x = x_0$) above the edges of the contact.

First, Miller and Singh (1994) introduced the tilt angle, that is the ratio of the vertical derivative ($\partial G/\partial z$) to the value of the total horizontal derivative (*THDR*), which is defined as:

$$TA\ (\phi) = \tan^{-1}\left(\frac{\partial G/\partial z}{THDR}\right) \qquad (5)$$

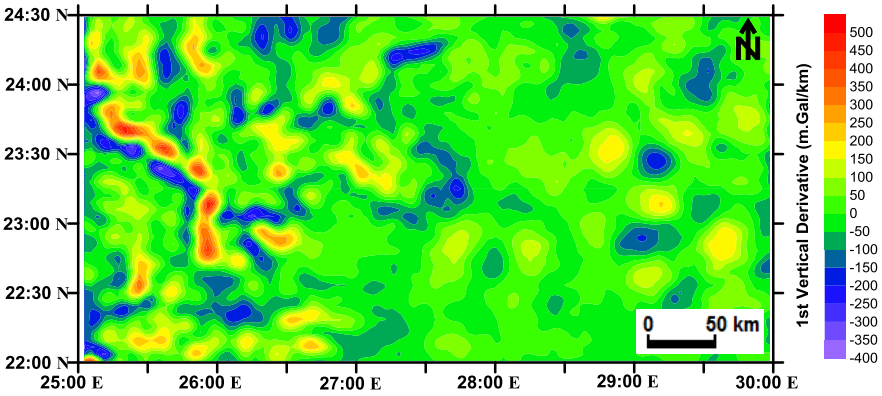

Figure (14): First vertical gravity gradient map produced from Figure 12 (Sedimentary section 1st V.D.).

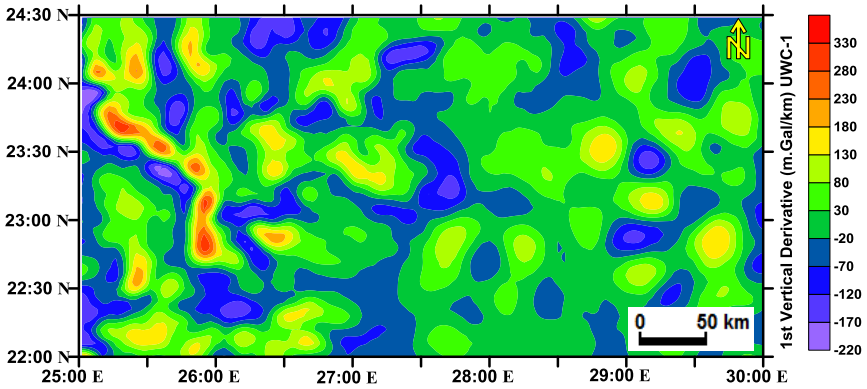

Figure (15): Upward continuation of the 1st Vertical Derivative at a lower altitude.

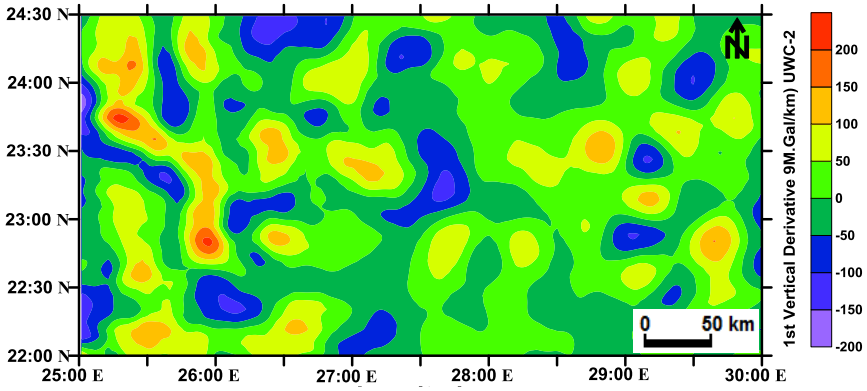

Figure (16): Upward continuation of the 1st Vertical Derivative at a higher altitude.

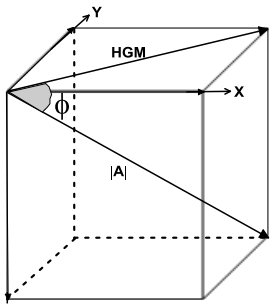

Figure (17): Schematic diagram showing the tilt angle"ϕ" "HGM" and |A| represent the horizontal gradient magnitude and analytic signal.

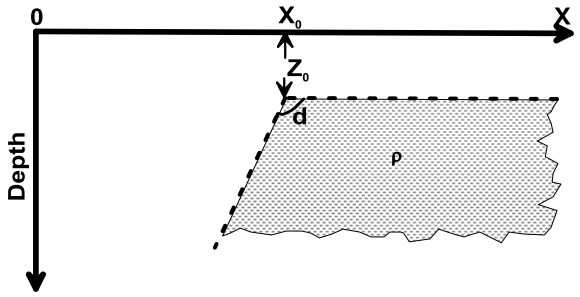

Figure (18): 2D sloping contact model, d is the dip (measured from the x-axis), z0 is the depth to the top of the contact, x_0 is the horizontal location, and ρ is the rock unit's density

Also, Verduzco et al. (2004) developed the tilt angle filter and redefined this filter as:

$$\text{TA}(\phi) = \tan^{-1}\left(\frac{\partial G/\partial z}{\sqrt{(\partial G/\partial x)^2 + (\partial G/\partial y)^2}}\right) \qquad (6)$$

Where: "*G*" is the magnetic or gravity field, and $\partial G/\partial x$, $\partial G/\partial y$and $\partial G/\partial z$ are the first derivatives of the field "*G*" in the x, y and z directions.

An important feature of the TA is that; the amplitudes of strong and weak anomalies can be balanced effectively, which is effective in allowing anomalies to be traced out along-strike, while being relatively insensitive to the depth of the source (Miller and Singh, 1994).Due to this, the TA has the equal attribute for different depth sources, and is able to detect the boundaries of deeper sources, which are often swamped in the larger responses of shallower sources. Verduzco et al. (2004) have demonstrated that, the TA values are restricted to values between $+\pi/2$ and $-\pi/2$ (+ 90° and− 90°), due to the natural property of the arc-tangent function. Added, if the density contrast is positive, the tilt angle value is positive when over the source, passes through zero when over or near the edge, where the vertical derivative is zero and the horizontal derivative is a maximum and is negative outside the source zone.

Note that, the zero contours of the TA delineate the spatial location of the edges of the models, responding well to the edge locations. The TA is useful in imaging the edges, although the models are located at the different depths.

Accordingly, **The Fourth Step** was evaluating the TA maps used in recognizing the horizontal locations and relative depths of the expected geologic contacts. The TA technique was implemented on the three data sets of the 1st VD without upward continuation, the 1st VD with lower upward continuation and the 1st VD with higher upward continuation. The results are illustrated in Figures (19, 20, and 21), respectively. Figure (22) is a tilt angle map of the basement complex showing the lithological variations rather than the structural dislocations.

And, Figure 23 shows the deduced structural lineaments from the tilt angle of the upward-continued maps (Figs. 20 & 21).

III.2.e- Total Horizontal Derivative of Tilt Angle

The horizontal derivative concept was discussed by many authors, among them, Ferreira et al (2011), Ferreira et al (2013) and many others. The total horizontal derivative of the tilt angle (TA-THDR) map (Figure 25) was further proposed by Thurston et al., (1997) to enhance the edges, and is calculated as follows:

For the grid data, the TA-THDR is (Verduzco et al., 2004):

$$\text{TA\_THDR} = \sqrt{\left(\frac{\partial TA}{\partial x}\right)^2 + \left(\frac{\partial TA}{\partial y}\right)^2} \qquad (7)$$

and for the profile data in the x direction:

$$\text{TA\_THDR} = \left|\frac{\partial TA}{\partial x}\right| \qquad (8)$$

The TA-THDR maxima are centered over the body edges, which include some narrower features before coalescing into a single peak. TA-THDR inherits the advantage of TA and is free from the constraints of the tilt angle of the geological body; therefore, it is better adapted for detecting the field source boundaries with any tilt angle. Figure 26 shows the interpreted lineaments from the THDR of TA map.

Roy et al (2017) have demonstrated that TA and its horizontal derivative are found to be sensitive to noise, while the upward continuation was proved to be an effective tool to handle the issue of noise contamination. Figure (27) is the lineaments' relative expected depth map, where, (H) points to relatively higher zones and (L) points to relatively lower zones. Number of arrows' segments is directly proportional to the expected lineament depth.

Figure 28 shows the combined fault elements deduced from T Abasement depth map and TA for the UWC map.

Figure 29 is a rose diagram showing the predominantly structural trends in the NNE-SSE, NW-SE, nearly E-W and NNW-SSE directions.

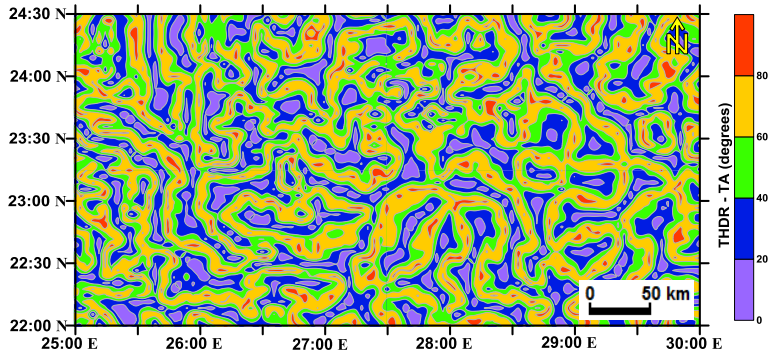

Figure 25: Total horizontal derivative of the tilt angle.

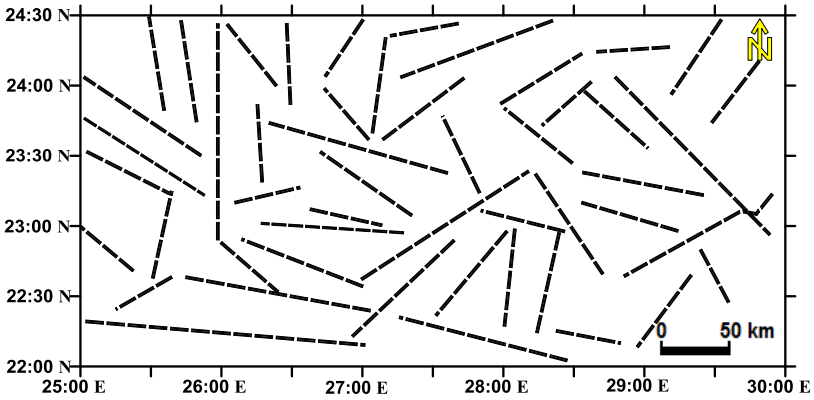

Figure 26: Interpreted lineaments from the THDR of TA map.

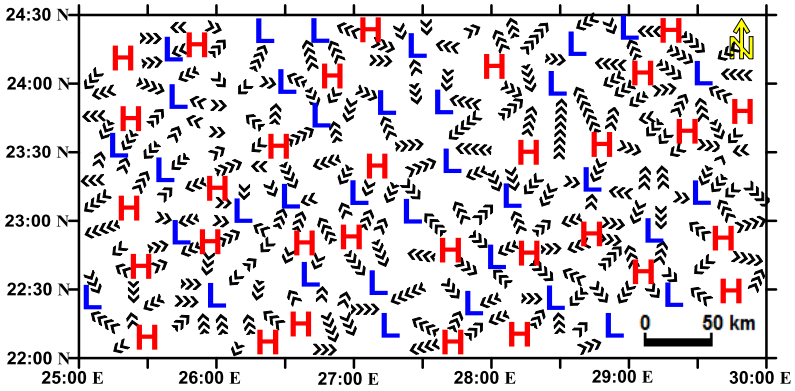

Figure 27: Lineaments' expected relative depth map. H=high zone& L=low zone. Number of arrows' segments is directly proportional to the expected lineament depth.

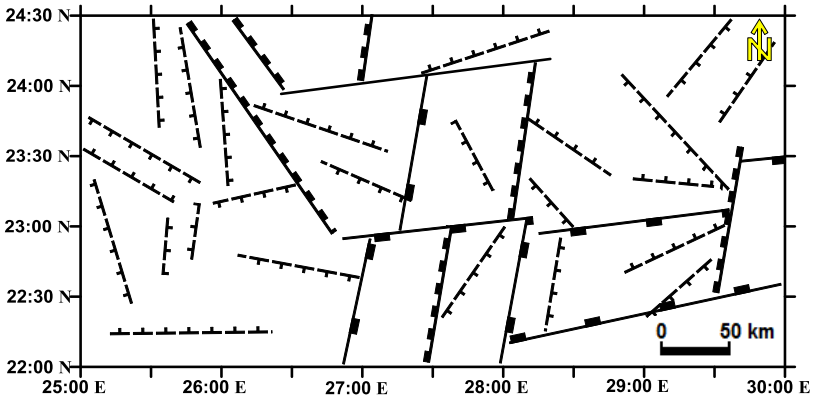

Figure (28): Combined expected fault elements of both TA basement map and UWC TA map.

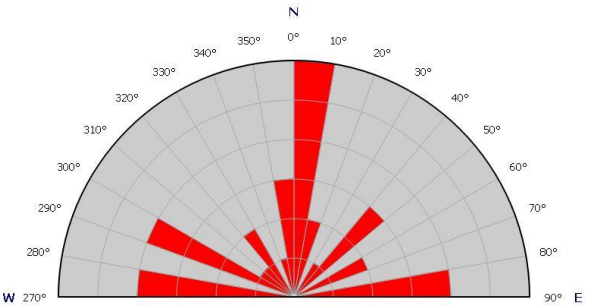

Figure (29): Rose diagram showing the predominant structural trends affecting the study area.

IV- CONCLUSIONS

The application of edge detection techniques on the available gravity data, of the far southwestern area of Egypt showed that, almost all filters exhibited predominantly NNE-SSE, NW-SE, nearly E-W and NNW-SSE structural trends

The Tilt Angle Maps (TAM), as obtained from the gravity vertical gradient in its simplest form assumes that, the source structures have vertical contacts. The tilt angle of the vertical gravity gradient is a very useful interpretation tool, since it provides a simple and clean image.

The technique tends to enhance mapping of the subtle gravity anomalies, and maximizes characterizing the geometrical contrast of the anomalous sources. The coherence of results indicates that the method produces satisfactory depth estimates under noise conditions.

The main advantage of this technique is that it enhances the amplitudes in areas with smooth anomalies, without sacrificing the long-wavelength information. Therefore, the spatial images of the TAM reflect different attributes of linear features, such as faults, contacts, and edges of basins and uplifts. The TAM and Edge Detection (ED) can be applied in the process of interactive interpretation of the gravity anomalies. While both methods have been able to delimit the edges of structural features in the sedimentary terrains, it is evident that, the TAM images have clearer indications of utility than those of the ED solutions. Because the analysis of TAM is only based on the contours of three angles (0, $\pi/2$ and $-\pi/2$ radians), the TAM images are easily interpreted by following these contours.

The TAM and ED images contain many details for detecting the edges of anomalous sources and some further analysis would improve the gravity interpretation. However, the TAM images should be compared with the ED solutions since the ED provides and helps to identify the source geometries. Thus, the ED confirms the results from the TAM under the assumption that, the edges of anomalous sources are caused by vertical contacts.

This correlation is the easiest way to confirm the horizontal locations and relative depths of the edges, especially when there is a lack of any geophysical data in the corresponding area.

The results obtained from this study provide valuable information for geologists and petroleum engineers to delineate the horizontal location of the buried faults, contacts and other structural and geological features.

ACKNOWLEDGMENT

My great appreciation is to the meritorious reviewers together with the Journal Editorial Board for their supportive comments in improving this first version of this manuscript.

REFERENCES

Abdelrahman, E.M., H.M. EI-Araby, T.M. EI-Araby, and E.R: Abo-Ezz (2003). A least-squares derivatives analysis of gravity anomalies due to faulted thin slabs. Geophysics 68 (2), 535-543.

Aboulela; H.A.M. (2012): Contribution of Satellite Altimetry Data in the Environmental Geophysical Investigation of the Northern Egyptian Continental Margin. International Journal of Geosciences, 3, 431-442

Alexander M., Prieto C., Radovich B. (2003): Basement Structural Analysis Key in Deep Shelf Play. The American oil and gas Reporter, no. 10.

Alkdagry; A.H.H. (2015): Subsurface structural mapping Melut Basin using satellite gravity data. Dissertation in Exploration Engineering, Sudan University of Science and Technology.

Ana C. Pedraza De Marchi, Marta E. Ghidella, Claudia N. Tocho (2014): Analysis of Different Methodologies to Calculate Bouguer Gravity Anomalies in the Argentine Continental Margin. Geosciences, Vol. 4 No. 2, 2014, pp. 33-41.

Beltrao, J.F, Silva J.B.C. and Costa J.C (1991): Robust polynomial fitting method for regional gravity estimation: Geophysics. doi: 10.1190/1.1442960.

Bonvalot, S., Balmino, G., Briais, A., Kuhn, M., Peyrefitte, A., Vales N., Biancale, R., Gabalda, G., Reinquin, F., Sarrailh, M., (2012). World Gravity Map. Commission for the Geological Map of the World. Eds. BGI-CGMW-CNES-IRD, Paris.

Braitenberg, C., Wienecke, S., and Wang, Y., (2006): Basement structures from satellite derived gravity field: South China Sea ridge. J. Geophys. Res. 111, B05407.

Burollet, P.F, (1963): Reconnaissance géologique dans le sud-est du bassin de Kufra. Inst. Francais Pétrole 18: 1537-1545.

Conoco-Corporation, L.T.D. (1987): Geological Map of South Western Desert Egypt, 1987, Scale 1:500.000, Sheet No. NF 53 NV, Gilf Kabeir Plateau, Egyptian General Petroleum Corporation, Cairo, 1987.-Cooper G .R.J.,

Cowan D.R., (2006): Enhancing potential field data using filters based on the local phase. Computers and Geosciences 32, 1585–1591.

Conoco-Corporation, (1987): Geological Map of South Western Desert Egypt, Scale 1500.000," Sheet No. NF 53 NV, Gilf Kabeir Plateau, Egyptian General Petroleum Corporation, Cairo, 1987

Cooper, G.R.J. (2003): Feature detection using sunshading, Comput. Geosci. 29, 941–948.
Cooper G.R.J. (2009): Balancing images of potential field data. Geophysics 74, L17–L20.

Cooper, G.R.J., Cowan D.R., (2008): Edge enhancement of potential-field data using normalized statistics. Geophysics 73 (3), H1–H4.

Cooper G.R.J., Cowan D.R., (2009): Terracing potential field data. Geophysical Prospecting, 57,1067–1071.

Nguyen Nhu, Trung & Lee, Sang-Mook & Que, Bui. (2004): Satellite Gravity Anomalies and Their Correlation with the Major Tectonic Features in the South China Sea. Gondwana Research. 7. 407-424. DOI: 10.1016/S1342-937X (05)70793-0.

Cordell L., Grauch V.J.S. (1985): Mapping basement magnetization zones fromaeromagnetic data in the San Juan Basin, New Mexico. In: Hinze, W.J. (Ed.), the Utility of Regional Gravity and Magnetic Anomaly Maps. Society of Exploration Geophysicists, Tulsa, Oklahoma, pp. 181-197.

El Ramly M.F. (1972): A new geological map for the basement rocks in the Eastern and south Western Deserts of Egypt. Annals of the Geological Survey of Egypt. Cairo.

El-Baz F., Boulos L., Breed C., Dardir A., Dowidar H., El-Etr H., Embabi N., Grolier M., Haynes V., Ibrahim M, Issawi B., Maxwell T., Mccauley J., Mchugh W., Moustafa A., and Yousif M., (1978): Journey to the Gilf El-Kebir and Uweinat, Southwest Egypt. Report.

Eshaghzadeh, A., (2014): Anomaly Edge Enhancement of Microgravity Data Using NormalizedStandard Deviation. Geodynamics Research International Bulletin, 2, XLVIII- LII.

Evjen H.M., (1936): The place of the vertical gradient in gravitational interpreta- tions. Geophysics 1, 127–136.

Ferreira F.J.F., de Castro L. G., Bongiolo A.B.S., de Souza J., and Romeiro M. A. T., (2011): Enhancement of the total horizontal gradient of magnetic anomalies using tilt derivatives: Part II-Application to real data: 81st Annual International Meeting, SEG, Expanded Abstracts, 887–891.

Ferreira F.J.F., de Souza J., Bongiolo, A.B.S. and de Castro L. G., (2013): Enhancement of the total horizontal gradient of magnetic anomalies using the tilt angle, Geophysics,78, J33–J41.

Fullea J., Fernandez M. and Zeyen H., (2008): FA2BOUG-A FORTRAN 90 code to compute Bouguer gravity anomalies from gridded free-air anomalies: Application to the Atlantic-Mediterranean transition zone, Computers & Geosciences, vol. 34, p. 1665-1681.

General Petroleum Company (GPC), 1984: Project of establishing the gravity map of Egypt.

Geosoft Inc. (1996): OASIS Montaj Version 4.0 User Guide. Geosoft Incorporated, Toronto.

Grant F.S. and West G.F. (1965): Interpretation theory in applied geophysics. New York, McGraw-Hill.

Gunn P.J., 1975. Linear transformations of gravity and magnetic fields, Geophys. Prospec. , 23, 300–312

Hackney R.I., and Featherstone W.E., (2003): Geodetic versus geophysical perspectives of the gravity anomaly. Geophys. J. Int., July 2003, v.154, p. 35-43

Hansen, R.O., Pawlowski, R.S., and WANG, X. (1987): Joint use of analytic signal and amplitude of horizontal gradient maxima for three-dimensional gravity data interpretation, 57th annual international management, Soc. Expl. Geophys., Expanded Abstracts 100–102.

Helal A.H. (1966): Jurassic plant microfossils from the subsurface of Kharga Oasis, Western Desert, Egypt. Paleontographica 117(A):83-98

Hood P.J., and Teskey D.J., (1989): Aeromagnetic gradiometer program of thegeological survey of Canada. Geophysics 54(8), 1012-1022.

Kedves M., (1971): Presence de types sporomorphes importants dans les sediment pre-quaternaires Egyptians. Acta Botanica Academiae Scietiarum Hungaricae 17:371-378

Klingele E.E., Marson I. and Kahle H.G. (1991): Automatic interpretation of gravity gradiometric data in two dimensions (Vertical gradients) Geophysical Prospecting 39: 407–434.

Klitzsch E. (1984): "Northwestern Sudan and Bordering Areas: Geological Development since Cambrian time", Sonderforschungsbereich 69, Results of Special Research Project Arid Areas, period 1981–1984, Berlin Verlag Von Dietrich Reimer

Klitzsch E. and Wycisk P. (1989): Carboniferous of northern Sudan and southern Egypt. XI Congres International de Stratigraphie et de géologie.

Klitzsch, E. and Wycisk, P. (1987) Geology of the sedimentary basin of northern Sudan and bordering areas. Berliner geowissenschaftliche Abhandlungen, A, 75, 1, pp. 97-136, Berlin.

Ma G. and Li L., (2012): Edge detection in potential fields with the normalized total horizontal derivative. Computers & Geosciences 41 (2012) 83–87.

Mahrholz W.W, (1965): Geological exploration of the Kufra region. Geological section, Ministry of Industry Libya, Tripoli. No. S: 1-76,

McGinnis, L.D., Wolf, M.G., Kohsmann, J.J., Ervin C. P (1979): Regional free air gravity anomalies

and tectonic observations in the United States. Journal of Geophysical Research. Volume 84, Issue B2, Pages 591–601

Miller H.G., Singh V., (1994): Potential field tilt - a new concept for location of potential field sources.Journal of Applied Geophysics. 32, 213–217.

Nabighian M. N., (1972): The analytical signal of 2D magnetic bodies with polygonal cross-section: Its properties and use for automated anomaly interpretation: Geophysics, 37, 507–517.

Nguyen Nhu Trung, Sang-Mook Lee, and Bui Cong Que (2004): Satellite Gravity Anomalies and Their Correlation with the Major Tectonic Features in the South China Sea. Gondwana Research, V. 7, No. 2, pp. 407-424

Oruç B, (2011): Edge Detection and Depth Estimation Using a Tilt Angle Map from Gravity Gradient Data of the Kozaklı-Central Anatolia Region, Turkey. Pure and Applied Geophysics, Volume 168, Number 10, Page 1769

Roy, P., Sai Krishnaveni, A. & Vinod Kumar, K. J. (2017). Geological evaluation of EIGEN-6C4 and GOCE derived gravity models in and around Karakoram shear zone, Leh, India. Geol Soc India. 90: 51-61. https://doi.org/10.1007/s12594-017-0663-2

Saad S.I. & Ghazaly G., (1976): Palynological studies in Nubia Sandstone from Kharga Oasis. Pollen et Spores. 18:407-470

Said R., (1962): The Geology of Egypt, Elsevier, Amsterdam and New York, 377 p,Said, R.: New light on the origin of the Qattara Depression. Bull. Soc. Geograph. Egypt, 33, (1960), 37-44.

Sandwell D.T. and Smith W.H.F. (1997): Marine gravity anomaly from Geosat and ERS 1 satellite altimetry. J. Geophy. Res., v. 102, pp. 10039-10054.

Thurston J.B., Smith R.S., (1997): Automatic conversion of magnetic data to depth, dip andsusceptibility contrast using the SPI method. Geophysics 62, 807–813.

Verduzco B., Fairhead J.D., Green C.M., (2004): New insights into magnetic derivatives forstructural mapping. The Leading Edge 23 (2), 116–119.

Wendorf F., (1977): Late Pleistocene and Recent climatic changes in the Egyptian Sahara. Geogri. J.143,2: 211-34.

Wijns C., Perez C., Kowalczyk P., (2005): Theta map: edge detection in magnetic data. Geophysics70 (4), 39–43.